ChemComm

COMMUNICATION

View Article Online
View Journal | View Issue

Cite this: *Chem. Commun.*, 2025, **61**, 913

Received 15th November 2024,
Accepted 5th December 2024

DOI: 10.1039/d4cc06083k

rsc.li/chemcomm

Sensitization experiments of ultrasmall gold nanoclusters: determination of triplet quantum yields and molar absorption coefficients†

Hayato Sakai,[a] Sunao Hiramatsu,[a] Aoi Akiyama,[b] Yuichi Negishi *[bc] and Taku Hasobe *[a]

We demonstrated for the first time the determination of triplet quantum yields and molar absorption coefficients of ultrasmall gold nanoclusters specifically $[Au_{25}(PET)_{18}]^-$ with phenylethanethiolate (PET) ligands using two sensitization experiments.

Recently, metal nanoclusters have attracted considerable interest in various basic and applied research fields owing to their size-dependent structures and properties derived from their discrete electronic structures.[1–12] In particular, ligand-protected ultrasmall metal nanoclusters exhibit characteristic molecular behaviours associated with the energy gap between the highest occupied molecular orbital (HOMO) and lowest unoccupied molecular orbital (LUMO).[13] For example, regarding $[Au_{25}(PET)_{18}]^-$ (denoted as $Au_{25}(PET)_{18}$) with phenylethanethiolate (PET) ligands, single-crystal X-ray diffraction demonstrated that $Au_{25}(PET)_{18}$ is composed of an icosahedral Au_{13} kernel and six $Au_2(PET)_3$ staple motifs on the surface.[14,15] The molecular behaviour of these metal nanoclusters is attributed to singlet or triplet excited states,[16] but the detailed excited-state dynamics associated with the molar absorption coefficients (ε_T) and quantum yields (Φ_T) in the triplet states are yet to be determined. The singlet–triplet (S_1–T_1) energy gaps (E_{S-T}) of ultrasmall gold nanoclusters such as Au_{25} clusters (*e.g.*, $E(S_1) = \sim 1.4$ eV and $E(T_1) = \sim 1.2$ eV) have been reported to be much smaller than those of organic materials according to theoretical calculations and spectroscopic measurements.[17,18] Thus, the values of $E(S_1)$ and $E(T_1)$ can be controlled simply and mainly by the number of metal atoms and types of ligands, making it much easier to establish a strategy for material design as compared to organic materials. Therefore, gold nanoclusters are useful for photo-functionalities based on absorption, emission,[19–24] and electron/energy transfer in the visible (red) and NIR regions, and are expected to be explored in various fields such as energy conversion, catalysis, electronics, and biomedical applications.[25–28]

The photophysical behaviours associated with triplet excited states (T_1) of ultrasmall gold nanoclusters (*e.g.*, Au_n: n = 25, 38) include phosphorescence emission through intersystem crossing (ISC),[19,20] reverse intersystem crossing (RISC)[29] and singlet oxygen ($^1O_2$) generation in oxygen-containing solutions.[30] Additionally, the bimolecular rate constant ($\sim 10^6$ M^{-1} s^{-1}) is extremely small, although the intermolecular triplet-triplet energy transfer (T-TEnT) from Au_n to organic chromophores was observed.[31] Time-resolved spectroscopy, such as transient absorption spectra (TAS) and emission lifetimes, suggested that TAS of Au_{25} from the longest lifetime component and photoluminescence decay at $\sim$1100 nm involve the excited state derived from the same T_1.[16,32–34] These lifetimes of Au_{25} (*ca.* 50–200 ns) are much shorter than those of the typical T_1 lifetimes of organic chromophores ($\sim$microsecond region). However, no attention has been paid to the determination of the ε_T and Φ_T of such gold nanoclusters. Although sensitization experiments using T-TEnT with an energy donor (a sensitizer) are useful for assigning the triplet TAS and corresponding ε_T values, the T_1 lifetimes of Au_n are extremely short. Accordingly, conventional methods are difficult to sufficiently evaluate.

Here we demonstrate two different sensitization experiments to evaluate the triplet character of $[Au_{25}(PET)_{18}]^-$ (denoted as $^3Au_{25}(PET)^*_{18}$) for the determination of the ε_T and Φ_T. First, the diffusion-controlled intermolecular T-TEnT from a sensitizer (C_{60}) to $Au_{25}(PET)_{18}$ ($\sim 10^{10}$ M^{-1} s^{-1}) was observed in toluene. Then, the diffusion-controlled quenching trend of $^3Au_{25}(PET)^*_{18}$ in O_2-saturated toluene ($\sim 10^{10}$ M^{-1} s^{-1}) demonstrated the intermolecular T-TEnT from $Au_{25}(PET)_{18}$ (energy donor) to $^3O_2$ (energy acceptor), yielding $^1O_2$ generation

[a] *Department of Chemistry, Faculty of Science and Technology, Keio University, Yokohama 223-8522, Japan. E-mail: hasobe@chem.keio.ac.jp*
[b] *Department of Applied Chemistry, Faculty of Science, Tokyo University of Science, 1-3 Kagurazaka, Shinjuku-ku, Tokyo 162-8601, Japan*
[c] *Institute of Multidisciplinary Research for Advanced Materials, Tohoku University, Katahira 2-1-1, Aoba-ku, Sendai 980-8577, Japan. E-mail: yuichi.negishi.a8@tohoku.ac.jp*

† Electronic supplementary information (ESI) available: Experimental section, synthesis, spectroscopic measurements. See DOI: https://doi.org/10.1039/d4cc06083k

with the triplet yield (Φ_T: 24%). Based on these results, the ε_T of $^3Au_{25}(PET)^*_{18}$ were successfully assigned. Additionally, the triplet behaviour of $Au_{38}(PET)_{24}$ was compared with $Au_{25}(PET)_{18}$.

The syntheses and characterization of $Au_{25}(PET)_{18}$ and $Au_{38}(PET)_{24}$ were performed according to the reported method (Schemes S1 and S2 and Fig. S1 and S2 and Table S1 in ESI†).[35,36] To determine the singlet and triplet energies ($E(S_1)$ and $E(T_1)$), we also measured luminescence spectra of $Au_{25}(PET)_{18}$ at low temperatures following the reported methods[20] (Fig. S2 and S3 in ESI†). Consequently, $E(S_1)$ and $E(T_1)$ of $Au_{25}(PET)_{18}$ were determined to be 1.5 eV and 1.2 eV, respectively. These values are comparable to the above-mentioned theoretical and experimental values of the related Au_{25}.[18,20] Additionally, the $E(S_1)$ and $E(T_1)$ of $Au_{38}(PET)_{24}$ should be slightly smaller than those of $Au_{25}(PET)_{18}$ according to previous report.[18]

According to previous reports,[16,37] the ISC pathways of $Au_{25}(PET)_{18}$ and $Au_{38}(PET)_{24}$ are expected to be extremely fast. To examine the singlet and triplet characters, femtosecond transient absorption spectra (fs-TAS) were systematically measured in toluene (Fig. 1 and Fig. S4–S10 in ESI†). Although the origin of the absorption properties is generally dependent on the excitation wavelengths, we mainly chose 650 nm because there was no significant difference in the triplet behaviours upon either 350 or 650 nm excitation (Fig. S4–S6, ESI†). In the case of $Au_{25}(PET)_{18}$, the ultrafast relaxation occurred within *ca.* 4.0 ps after laser-pulse excitation (Fig. 1A and B), and long-lived excited species, extending from the visible to near-infrared (NIR) region (*ca.* 400–900 nm), remained within the measurement time-range of fs-TAS up to ~6.0 ns. Assuming that this process is associated with ISC, the corresponding species-associated spectra (SAS) of $Au_{25}(PET)_{18}$ were analysed by target analysis (see: Fig. S11 and S12 in ESI†),[38] yielding the SAS of S_1 and T_1 (Fig. 1C). The time-dependent concentration profiles (inset figure in Fig. 1C) demonstrate the ultrafast deactivation process. Note that the behaviour of the initial species is beyond the time-resolution of fs-TAS. The first species (trace a) and second species (trace b) should be attributed to S_1 and T_1, respectively. The longer and second species continue to be undecayed in the above-mentioned time-range (~6 ns) (Fig. S4 in ESI†). Regarding $Au_{38}(PET)_{24}$, a similar relaxation process occurs within *ca.* 1 ps, whereas second and longer species decayed with the lifetime of ~6 ns. This is in sharp contrast with $Au_{25}(PET)_{18}$. Noted that the singlet character derived from RISC process from T_1 to S_1 could not be obtained in $Au_{25}(PET)_{18}$ and $Au_{38}(PET)_{24}$ (see: the temperature-dependent fs-TAS in Fig. S13 in ESI†).

To further observe the longer timescale in $Au_{25}(PET)_{18}$, we also measured picosecond transient absorption spectra (ps-TAS) of $Au_{25}(PET)_{18}$ (Fig. S14 and S15 in ESI†). The resulting excited species of $Au_{25}(PET)_{18}$ remained and the lifetime was calculated to be 160 ns at 298 K. No excitation wavelength-dependent spectral changes of S_1 were observed for both $Au_{25}(PET)_{18}$ and $Au_{38}(PET)_{24}$ (Fig. S14–S17 in ESI†). From these results, triplet lifetimes of 160 ns for $Au_{25}(PET)_{18}$ and 5.0 ns for $Au_{38}(PET)_{24}$ were predicted, which are much shorter than those of typical organic molecules.

Thus, the above-mentioned fs-TAS allowed us to predict the triplet TAS of Au_n (n = 25, 38), although it is necessary to confirm whether these predictions are essentially correct or not. Therefore, we first observed triplet TAS of $Au_{25}(PET)_{18}$ using T-TEnT with a sensitizer (C_{60}). Fig. 2A presents ps-TAS in a mixed toluene solution of C_{60} and $Au_{25}(PET)_{18}$. The excitation wavelength chosen was 355 nm to mainly excite C_{60}. The molar ratio between C_{60} and $Au_{25}(PET)_{18}$ was also optimized after preliminary experiments in which the ps-TAS were measured by varying the ratios. After laser-pulse excitation, we initially observed the triplet spectrum of C_{60} at *ca.* 750 nm. Note that 355 nm excitation includes a small amount of absorption in $Au_{25}(PET)_{18}$, resulting in the appearance of $^3Au_{25}(PET)^*_{18}$ due to the direct excitation of $Au_{25}(PET)_{18}$ in addition to $^3Au_{25}(PET)^*_{18}$ produced by T-TEnT from C_{60} (Fig. 2A and Fig. S2 in ESI†). Another serious problem arises from the fact that the lifetime of $^3Au_{25}(PET)^*_{18}$ is much shorter than that of $^3C^*_{60}$. Therefore, it is difficult to distinguish the triplet absorption spectrum of $Au_{25}(PET)_{18}$ by the direct excitation from that by intermolecular T-TEnT from C_{60}. Although the ε_T cannot be determined by this method, the strong quenching process of $^3C^*_{60}$ was clearly observed at 750 nm

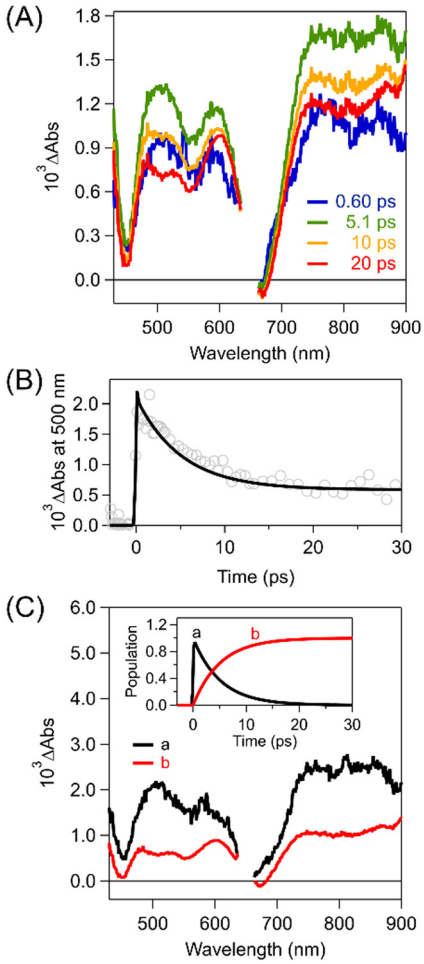

Fig. 1 (A) fs-TAS of $Au_{25}(PET)_{18}$ in toluene (λ_{ex}: 650 nm) and (B) the time profile at 500 nm (298 K). (C) Species-associated spectra (SAS) of (a) first (black) and (b) second (red) species. Inset: The time-dependent concentration profiles of first and second species.

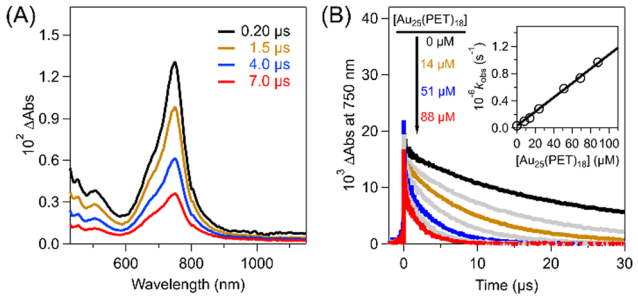

Fig. 2 (A) ps-TAS of C_{60} (32 μM) in the presence of $Au_{25}(PET)_{18}$ (20 μM) in toluene (298 K). λ_{ex}: 355 nm. (B) The corresponding time-profiles at 750 nm in the presence of different concentrations of $Au_{25}(PET)_{18}$. Inset: Pseudo-first order plot of k_{obs} monitored at 750 nm *versus* concentrations of $Au_{25}(PET)_{18}$.

(Fig. 2B). The time profile at 750 nm showed the significant quenching of $^3C_{60}^*$ with increasing the concentrations of $Au_{25}(PET)_{18}$. Fig. 2C also shows a linear plot of the observed decay rate constants (k_{obs}) at 750 nm based on the concentrations of $Au_{25}(PET)_{18}$. From the slope of the linear plot, the second-order rate constant of intermolecular T-TEnT from C_{60} to $Au_{25}(PET)_{18}$ was calculated to be 1.0×10^{10} M^{-1} s^{-1}. This is quite similar to the diffusion-limited value in toluene (k_{diff}: 1.1×10^{10} M^{-1} s^{-1}).[39] The similar photophysical trend of $Au_{38}(PET)_{24}$ was successfully observed (Fig. S18 in ESI†). These results clearly demonstrate the triplet characters of $Au_{25}(PET)_{18}$ and $Au_{38}(PET)_{24}$.

Then, another way to reveal the triplet character of Au_n involves a sensitization experiment in oxygen-saturated toluene because of the occurrence of intermolecular T-TEnT from Au_n to the molecular oxygen ($^3O_2$). In addition to the $^3O_2$- and Ar-saturated toluene solutions, air-saturated (21% $^3O_2$)[40] toluene solution was prepared according to the established method.[41] Fig. 3A shows ps-TAS of $Au_{25}(PET)_{18}$ in $^3O_2$-saturated toluene. Comparing these triplet absorption spectra with ps-TAS of $Au_{25}(PET)_{18}$ in Ar-saturated toluene (Fig. S14 and S15 in ESI†), no change in shape was observed. Fig. 3B shows strong decays in $^3O_2$-saturated and air-saturated toluenes compared to that in Ar-saturated toluene. These resulted in the occurrence of intermolecular T-TEnT because the triplet lifetimes in $^3O_2$-saturated (τ_T: 47 ns) and air-saturated (τ_T: 120 ns) toluenes were much shorter than that in Ar-saturated toluene (τ_T: 160 ns). Since there is a linear relationship between k_{obs} and $^3O_2$ concentrations, the second-order rate constant can be calculated to be 1.0×10^{10} M^{-1} s^{-1}. This is very close to the above-mentioned k_{diff} in toluene, which is in sharp contrast with the lack of quenching of $^3Au_{38}(PET)_{24}^*$ with $^3O_2$ (Fig. S19 in ESI†). At the saturated oxygen concentration in toluene (~10 mM), the decay rate constant (k_d) of $^3Au_{25}(PET)_{18}^*$ with $^3O_2$ was determined to be 1.0×10^8 s^{-1}. This is nearly two orders of magnitude greater than the rate constant of the triplet deactivation process of $Au_{25}(PET)_{18}$ (1/(160 ns) = 6.3×10^6 s^{-1}), whereas the k_d of $^3Au_{38}(PET)_{24}^*$ with $^3O_2$ should be smaller than that of $Au_{25}(PET)_{18}$ (1/(5.0 ns) = 2.0×10^8 s^{-1}). As a result, we can conclude that quantitative T-TEnT occurs between $^3Au_{25}(PET)_{18}^*$ and $^3O_2$.

The above-mentioned quantitative intermolecular T-TEnT from $Au_{25}(PET)_{18}$ to $^3O_2$ resulted in $^1O_2$ generation for evaluations of the Φ_T. To examine the Φ_T of $Au_{25}(PET)_{18}$ *via* ISC, we employed $^1O_2$ luminescence measurements using intermolecular T-TEnT from $Au_{25}(PET)_{18}$ to $^3O_2$ in $^3O_2$-saturated toluene at excitation wavelengths of 350 nm (Fig. 4A) and 650 nm (Fig. S20 in ESI†). By using intermolecular T-TEnT, we detected $^1O_2$ luminescence at *ca.* 1270 nm, assuming negligible quenching processes from S_1. The Φ_T of $Au_{25}(PET)_{18}$ was calculated based on the reference compound: C_{60} (Φ_T: 100%).[42] Consequently, the Φ_T of $Au_{25}(PET)_{18}$ (λ_{ex}: 350 nm) was determined to be 24 ± 1.8%. Additionally, the Φ_T of $Au_{25}(PET)_{18}$ (λ_{ex}: 650 nm) is 24 ± 2.2%, and these values does not depend on the excitation wavelengths (Tables S2–S4 in ESI†). In contrast, in the case of $Au_{38}(PET)_{24}$, no T-TEnT occurred, as discussed above. Thus, no $^1O_2$ peak at 1270 nm was observed in toluene (Fig. S21 in ESI†). The relatively small Φ_T of $Au_{25}(PET)_{18}$ is likely attributable to the nonradiative process from S_1 based on vibrational motion (*vide infra*). Based on the above Φ_T and ps-TAS of $Au_{25}(PET)_{18}$, the ε_T were obtained (Fig. 4B, calculation process in ESI†) together with the kinetic parameters (Table 1).

To further examine the detailed dynamics of $^3Au_{25}(PET)_{18}^*$, we also measured the temperature-dependent ps-TAS (Fig. S22 in ESI†). Although the T_1 lifetimes increased with decreasing temperatures, the RISC process was negligible considering the single-exponential decay curves of $^3Au_{25}(PET)_{18}^*$ together with

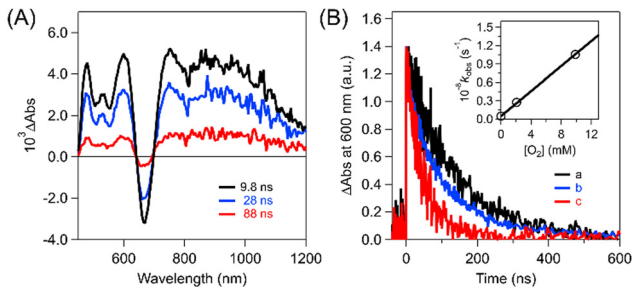

Fig. 3 (A) ps-TAS of $Au_{25}(PET)_{18}$ in O_2-saturated toluene (λ_{ex}: 355 nm) (298 K). (B) The time profiles at 600 nm in (a) Ar-saturated, (b) air-saturated (21% $^3O_2$), (c) $^3O_2$-saturated toluene. Inset: Pseudo-first order plot of k_{obs} monitored at 600 nm *vs.* $^3O_2$ concentrations.

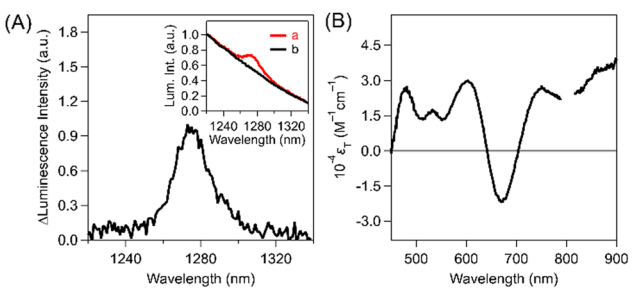

Fig. 4 (A) A luminescence differential spectrum of $Au_{25}(PET)_{18}$ in $^3O_2$-saturated toluene (298 K). The inset shows the parent luminescence spectra of $Au_{25}(PET)_{18}$ in (a) O_2- and (b) Ar-saturated toluenes. λ_{ex}: 350 nm. (B) The estimated ε_T values of $Au_{25}(PET)_{18}$ in toluene.

Table 1 Summarized photophysical parameters in toluene at room temperature (298 K)

	τ_S[a] ps	τ_T[b] ns	Φ_T[c] %	$k_{EnT} \times 10^{-9}$[d] M^{-1} s^{-1}	$k_{EnT} \times 10^{-9}$[e] M^{-1} s^{-1}
$Au_{25}(PET)_{18}$	4.0	160	24	10	10
$Au_{38}(PET)_{24}$	0.87	5.0	—	9.9	—

[a] Estimated by luminescence spectra. [b] Estimated by target analysis of fs-TAS. [c] Estimated by $^1O_2$ generation. [d] T-TEnT from C_{60} to Au_n (n = 25, 38). [e] T-TEnT from Au_n to $^3O_2$.

the above-mentioned S_1–T_1 gap of $Au_{25}(PET)_{18}$ (~0.3 eV). This energy gap is much larger than those of the reported Au_n with observations of RISC (~0.03 eV).[29] Hence, considering the above results of the temperature-dependent fs-TAS (Fig. S13 in ESI†) and ps-TAS, the origin of the changes in the excited lifetimes of the singlet and triplet states in temperature-dependent experiments is mainly due to the vibrational motions originating from Au_{13} kernel and/or six $Au_2(PET)_3$ staple motifs. This should be associated with the small Φ_T.[43] The proposed excited-state dynamics of $Au_{25}(PET)_{18}$ is also shown in Fig. S23 in in ESI.†

In conclusion, we demonstrated the triplet behavior of ultrasmall gold nanoclusters together with the determination of the Φ_T and ε_T using sensitization experiments. The simple and easy control of excited states in metal nanoclusters will stimulate basic and applied researches on excited triplet states in the future.

This work was partially supported by JSPS KAKENHI Grant-in-Aid for Transformative Research Areas, ''Materials Science of Meso-Hierarchy''(JP23H04876 to T. H.).

Data availability

The data supporting this article have been included as part of the ESI.†

Conflicts of interest

There are no conflicts to declare.

Notes and references

1 P. D. Jadzinsky, G. Calero, C. J. Ackerson, D. A. Bushnell and R. D. Kornberg, *Science*, 2007, **318**, 430–433.
2 R. W. Murray, *Chem. Rev.*, 2008, **108**, 2688–2720.
3 R. Jin, C. Zeng, M. Zhou and Y. Chen, *Chem. Rev.*, 2016, **116**, 10346–10413.
4 E. C. Dreaden, A. M. Alkilany, X. Huang, C. J. Murphy and M. A. El-Sayed, *Chem. Soc. Rev.*, 2012, **41**, 2740–2779.
5 A. Desireddy, B. E. Conn, J. Guo, B. Yoon, R. N. Barnett, B. M. Monahan, K. Kirschbaum, W. P. Griffith, R. L. Whetten, U. Landman and T. P. Bigioni, *Nature*, 2013, **501**, 399–402.
6 Y. Li, M. Zhou, Y. Song, T. Higaki, H. Wang and R. Jin, *Nature*, 2021, **594**, 380–384.
7 M. A. Abbas, P. V. Kamat and J. H. Bang, *ACS Energy Lett.*, 2018, **3**, 840–854.
8 S. Antonello, N. V. Perera, M. Ruzzi, J. A. Gascón and F. Maran, *J. Am. Chem. Soc.*, 2013, **135**, 15585–15594.
9 S. H. Yau, O. Varnavski and T. Goodson, III, *Acc. Chem. Res.*, 2013, **46**, 1506–1516.
10 T. Saegusa, H. Sakai, H. Nagashima, Y. Kobori, N. V. Tkachenko and T. Hasobe, *J. Am. Chem. Soc.*, 2019, **141**, 14720–14727.
11 W. Fei, S. Antonello, T. Dainese, A. Dolmella, M. Lahtinen, K. Rissanen, A. Venzo and F. Maran, *J. Am. Chem. Soc.*, 2019, **141**, 16033–16045.
12 Q. Yao, T. Chen, X. Yuan and J. Xie, *Acc. Chem. Res.*, 2018, **51**, 1338–1348.
13 Y. Negishi, T. Nakazaki, S. Malola, S. Takano, Y. Niihori, W. Kurashige, S. Yamazoe, T. Tsukuda and H. Häkkinen, *J. Am. Chem. Soc.*, 2015, **137**, 1206–1212.
14 M. Zhu, C. M. Aikens, F. J. Hollander, G. C. Schatz and R. Jin, *J. Am. Chem. Soc.*, 2008, **130**, 5883–5885.
15 M. W. Heaven, A. Dass, P. S. White, K. M. Holt and R. W. Murray, *J. Am. Chem. Soc.*, 2008, **130**, 3754–3755.
16 Z. Liu, M. Zhou, L. Luo, Y. Wang, E. Kahng and R. Jin, *J. Am. Chem. Soc.*, 2023, **145**, 19969–19981.
17 X.-S. Han, X. Luan, H.-F. Su, J.-J. Li, S.-F. Yuan, Z. Lei, Y. Pei and Q.-M. Wang, *Angew. Chem., Int. Ed.*, 2020, **59**, 2309–2312.
18 P. N. Day, R. Pachter, K. A. Nguyen and R. Jin, *J. Phys. Chem. A*, 2019, **123**, 6472–6481.
19 M. Sugiuchi, J. Maeba, N. Okubo, M. Iwamura, K. Nozaki and K. Konishi, *J. Am. Chem. Soc.*, 2017, **139**, 17731–17734.
20 Z. Wu, Q. Yao, O. J. H. Chai, N. Ding, W. Xu, S. Zang and J. Xie, *Angew. Chem., Int. Ed.*, 2020, **59**, 9934–9939.
21 M. Zhou and Y. Song, *J. Phys. Chem. Lett.*, 2021, **12**, 1514–1519.
22 S. Sharma, K. Kaushik, A. Salam, R. Garg, J. Mondal, R. Lamba, M. Kaur and C. K. Nandi, *ACS Appl. Nano Mater.*, 2024, **7**, 32–60.
23 W.-Q. Shi, L. Zeng, R.-L. He, X.-S. Han, Z.-J. Guan, M. Zhou and Q.-M. Wang, *Science*, 2024, **383**, 326–330.
24 K. L. D. M. Weerawardene and C. M. Aikens, *J. Am. Chem. Soc.*, 2016, **138**, 11202–11210.
25 T. Kawawaki, Y. Kataoka, M. Hirata, Y. Iwamatsu, S. Hossain and Y. Negishi, *Nanoscale Horiz.*, 2021, **6**, 409–448.
26 L. Liu and A. Corma, *Chem. Rev.*, 2018, **118**, 4981–5079.
27 Y. Du, H. Sheng, D. Astruc and M. Zhu, *Chem. Rev.*, 2020, **120**, 526–622.
28 Y.-S. Chen and P. V. Kamat, *J. Am. Chem. Soc.*, 2014, **136**, 6075–6082.
29 X. Wen, P. Yu, Y.-R. Toh, A.-C. Hsu, Y.-C. Lee and J. Tang, *J. Phys. Chem. C*, 2012, **116**, 19032–19038.
30 H. Kawasaki, S. Kumar, G. Li, C. Zeng, D. R. Kauffman, J. Yoshimoto, Y. Iwasaki and R. Jin, *Chem. Mater.*, 2014, **26**, 2777–2788.
31 M. Mitsui, Y. Wada, R. Kishii, D. Arima and Y. Niihori, *Nanoscale*, 2022, **14**, 7974–7979.
32 M. Zhou and R. Jin, *Annu. Rev. Phys. Chem.*, 2021, **72**, 121–142.
33 K. G. Stamplecoskie and P. V. Kamat, *J. Am. Chem. Soc.*, 2014, **136**, 11093–11099.
34 M. Zhou, C. Yao, M. Y. Sfeir, T. Higaki, Z. Wu and R. Jin, *J. Phys. Chem. C*, 2018, **122**, 13435–13442.
35 X. Kang, H. Chong and M. Zhu, *Nanoscale*, 2018, **10**, 10758–10834.
36 H. Qian, Y. Zhu and R. Jin, *ACS Nano*, 2009, **3**, 3795–3803.
37 T. D. Green and K. L. Knappenberger, *Nanoscale*, 2012, **4**, 4111–4118.
38 J. J. Snellenburg, S. Laptenok, R. Seger, K. M. Mullen and I. H. M. van Stokkum, *J. Stat. Software*, 2012, **49**, 1–22.
39 N. J. Turro, V. Ramamurthy and J. Scaiano, *Modern Molecular Photochemistry of Organic Molecules*, University Science Books, 2010.
40 M. Motalti, A. Credi, L. Prodi and M. T. Gandolfi, *Handbook of Photochemistry*, CRC Press, Boca Raton, 3rd edn, 2006.
41 S. Fukuzumi, H. Imahori, H. Yamada, M. E. El-Khouly, M. Fujitsuka, O. Ito and D. M. Guldi, *J. Am. Chem. Soc.*, 2001, **123**, 2571–2575.
42 D. K. Palit, A. V. Sapre, J. P. Mittal and C. N. R. Rao, *Chem. Phys. Lett.*, 1992, **195**, 1–6.
43 K. Kwak, V. D. Thanthirige, K. Pyo, D. Lee and G. Ramakrishna, *J. Phys. Chem. Lett.*, 2017, **8**, 4898–4905.

